AFRL-RV-PS-
TR-2012-0083

NEXT GENERATION, WAVEFORM BASED 3-DIMENSIONAL MODELS & METRICS TO IMPROVE NUCLEAR EXPLOSION MONITORING IN THE MIDDLE EAST

Brian Savage, et al.

University of Rhode Island
317 Woodward Hall
9 East Alumni Ave
Kingston, RI 02881

20 April 2012

Final Report

AIR FORCE RESEARCH LABORATORY
Space Vehicles Directorate
3550 Aberdeen Ave SE
AIR FORCE MATERIEL COMMAND
KIRTLAND AIR FORCE BASE, NM 87117-5776

DTIC COPY

NOTICE AND SIGNATURE PAGE

Using Government drawings, specifications, or other data included in this document for any purpose other than Government procurement does not in any way obligate the U.S. Government. The fact that the Government formulated or supplied the drawings, specifications, or other data does not license the holder or any other person or corporation; or convey any rights or permission to manufacture, use, or sell any patented invention that may relate to them.

This report was cleared for public release by the 377 ABW Public Affairs Office and is available to the general public, including foreign nationals. Copies may be obtained from the Defense Technical Information Center (DTIC) (http://www.dtic.mil).

AFRL-RV-PS-TR-2012-0083 HAS BEEN REVIEWED AND IS APPROVED FOR PUBLICATION IN ACCORDANCE WITH ASSIGNED DISTRIBUTION STATEMENT.

//signed//	//signed//
Robert J. Raistrick	Joel B. Mozer
RVBYE, Program Manager	RVB, Chief

This report is published in the interest of scientific and technical information exchange, and its publication does not constitute the Government's approval or disapproval of its ideas or findings.

Approved for public release; distribution is unlimited.

REPORT DOCUMENTATION PAGE

Form Approved
OMB No. 0704-0188

1. REPORT DATE *(DD-MM-YYYY)*	2. REPORT TYPE	3. DATES COVERED *(From - To)*
20-04-2012	Final Report	25 Jan 2008 to 25 Jan 2012

4. TITLE AND SUBTITLE
Next Generation, Waveform Based 3-Dimensional Models & Metrics to Improve Nuclear Explosion Monitoring in the Middle East

5a. CONTRACT NUMBER
FA8718-08-C-0009

5b. GRANT NUMBER

5c. PROGRAM ELEMENT NUMBER
62601F

6. AUTHOR(S)
Brian Savage, Daniel Peter, Brian M. Covellone, Arthur Rodgers, and Jeroen Tromp

5d. PROJECT NUMBER
1010

5e. TASK NUMBER
PPM00004583

5f. WORK UNIT NUMBER
EF004083

7. PERFORMING ORGANIZATION NAME(S) AND ADDRESS(ES)
University of Rhode Island
317 Woodward Hall
9 East Alumni Ave
Kingston, RI 02881

8. PERFORMING ORGANIZATION REPORT NUMBER

9. SPONSORING / MONITORING AGENCY NAME(S) AND ADDRESS(ES)
Air Force Research Laboratory
Space Vehicles Directorate
3550 Aberdeen Ave SE
Kirtland AFB, NM 87117-5776

10. SPONSOR/MONITOR'S ACRONYM(S)
AFRL/RVBYE

11. SPONSOR/MONITOR'S REPORT NUMBER(S)
AFRL-RV-PS-TR-2012-0083

12. DISTRIBUTION / AVAILABILITY STATEMENT

Approved for public release; distribution is unlimited. (377ABW-2011-1069 dtd 22 July 2011).

13. SUPPLEMENTARY NOTES
Additional support from Princeton University, Princeton, NJ 08540; Lawrence Livermore National Laboratory, Ground-Based Nuclear Explosion Monitoring Program, 7000 East Ave, L-205, Livermore, CA 94551

14. ABSTRACT

Improvements to the current Middle East wave-speed model with full waveforms require confidence in sources and recordings, along with a methodology to iteratively improve the model and reduce its minimum period. The mismatch between recordings of seismic waves traversing the region from Tibet to the Red Sea compared to synthetics from the current iteration model is the principal metric in improving the current wave-speed model. After the sources were evaluated, regions requiring refinement were highlighted using adjoint tomography methods based on spectral-element simulations. Inversion results demonstrate that the iterative nature of the adjoint tomography primarily improves the travel-time variations between synthetics and data, with less of an improvement to the waveform amplitudes. Iterative improvements also significantly increase anomaly strength while sharpening the anomaly edges to create stronger and more pronounced tectonic structures. The results presented here, while accurate at intermediate periods, require the addition of attenuation tomography and transverse isotropy without a vertical symmetry axis to further reduce the minimum period to that of travel-time tomography models.

15. SUBJECT TERMS
Seismic velocity, seismic attenuation, adjoint tomography, finite-frequency wave propagation, transverse isotropy, full waveform

16. SECURITY CLASSIFICATION OF:			17. LIMITATION OF ABSTRACT	18. NUMBER OF PAGES	19a. NAME OF RESPONSIBLE PERSON
a. REPORT	b. ABSTRACT	c. THIS PAGE			Robert Raistrick
UNCLASSIFIED	UNCLASSIFIED	UNCLASSIFIED	UNLIMITED	24	19b. TELEPHONE NUMBER *(include area code)*

This page is intentionally left blank.

Table of Contents

List of Figures

1. INTRODUCTION AND BACKGROUND

Improved 3D wave speed models of the greater Middle East, from the Turkish Plateau to the eastern edge of Tibet (Figure 1), enhances our ability to discriminate between natural and man-made events, locate these events, identify source depths, and determine magnitudes using waveform based methodologies. Current wave-speed models of the Middle East are improved through an adjoint tomography method [1] applied to seismic phase and amplitude data. An initial step towards the adjoint tomography model requires the development of a database of relocated and well-characterized sources and waveforms. The adjoint tomography method [1] uses full seismic waveforms as a measure of misfit of the current model iteration. Differences between data and synthetics are used to create adjoint sources and generate sensitivity kernels required to update the wave-speed model. The adjoint tomography model was built on the foundation of the seismic waveform database and finite-frequency wave propagation, and will be distributed to the community

Improvements to the 3D wave speed model for the Middle East using the adjoint tomography method, exploits the full seismic waveform, including amplitude and phase. Due to these requirements of improving an existing 3D model and using seismic waveform data, synthetic data need to be accurate for the chosen 3D wave speed model and the sources, e.g. initial event conditions need to be precise when comparing to real sources or events.

To assess the precision of our synthetic sources, events were re-inverted in 1D and 3D wave-speed models and agree fairly well with currently available solutions. Use of a 3D model further improves the waveform fit between data and synthetics, reduces the overall error of the CMT solution, provides a means to include shorter period arrivals, and improves most metrics of waveform fit.

Following source re-interpretation, the 3D wave speed model was updated using adjoint tomographic methods. The power of the methodology allows for incorporation of true, physics-based, wavefield propagation to localize errors in the wave speed model. Once errors are localized and identified the model can be updated and another iteration is possible. Final iterations for the Middle East 3D wave speed model amplify and sharpen wave-speed anomalies while increasing the predictive capabilities at periods of 20 seconds and longer for surface waves and 14 seconds and longer for body waves. This results in a wave-speed model with a resolution of about 60 km.

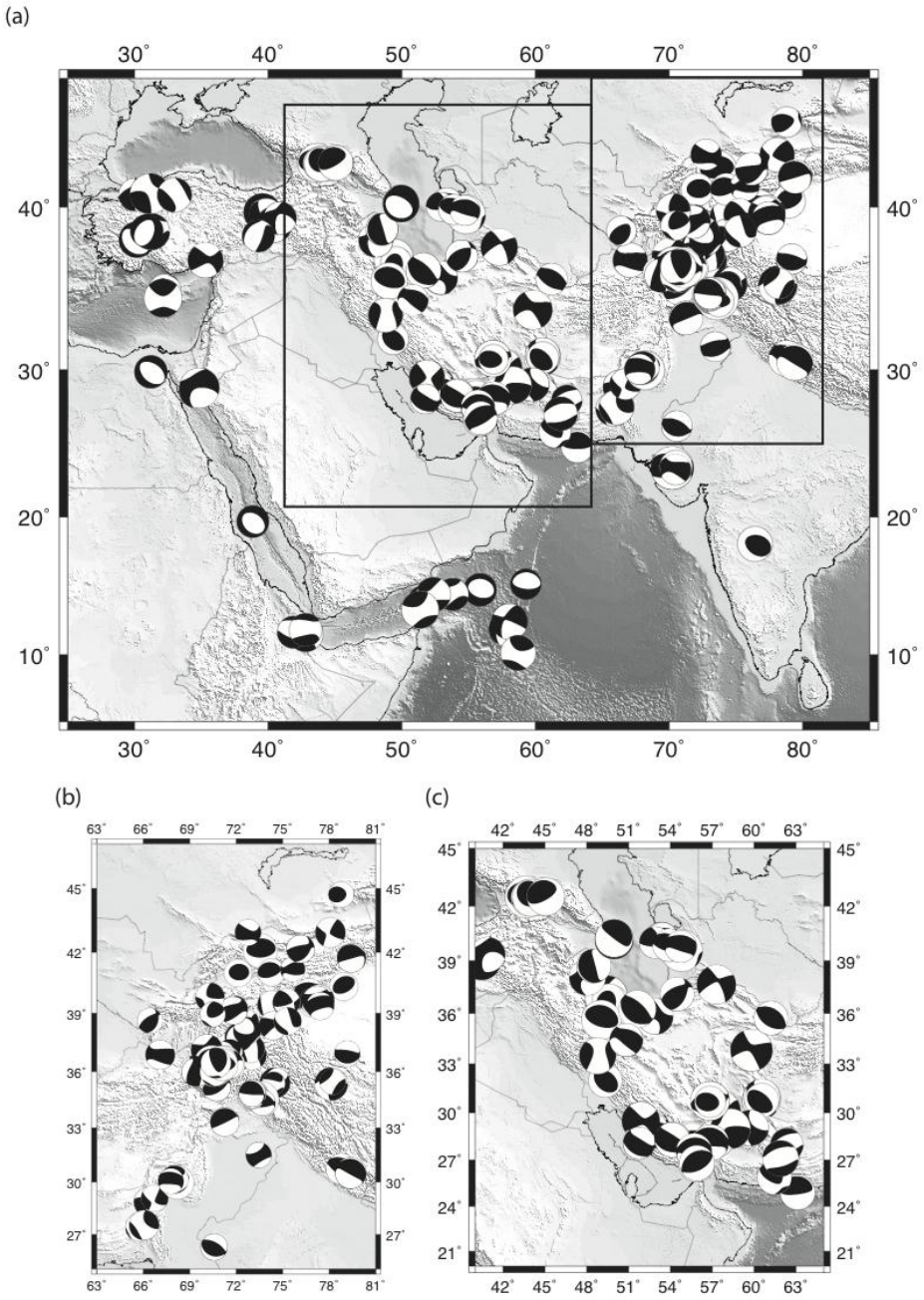

Figure 1. Map of Re-Characterized Events in the Middle East

2. METHODS, ASSUMPTIONS, AND PROCEDURES

The adjoint tomographic inversion is a two-step procedure where a source re-interpretation is first performed to develop a more precise realization of the events within the region. This is followed by an iterative 3D wave speed inversion driven by adjoint methods.

2.1. Event Re-Characterization

Within the Middle East approximately 200 events were re-characterized using the Moment Tensor (MT) inversion methodology of [2] and both the 1D PREM model [3] and a 3D wave-speed model (S2.9EA) [4] at periods of 25-125 seconds and of 60-125 seconds. A map of all available stations and events are shown in Figure 1. Initially, the procedures for processing large amounts of data, comparing the data to synthetics, and reevaluating the source parameters and locations needed to be assessed and streamlined. This development was accomplished through the use of a 1D wave-speed model and long-period modeling, and needed to be straightforward and nimble enough to avoid problematic areas, as the initial 3D event re-evaluation requires more demanding computational efforts. Problematic events and stations were subsequently screened out within this procedure before building the final waveform dataset. Problematic stations and waveforms with dropouts and poorly characterized amplitude responses can negatively influence a MT inversion, and these stations were removed before any 3D MT inversion or adjoint inversions were performed. Along with the development of a semi-automated procedure, the data were evaluated and bad quality data were omitted from the entire source and wave speed improvement procedure. The full inversion procedure we followed is detailed in [5] including the evaluation function and efforts to assess the solution stability.

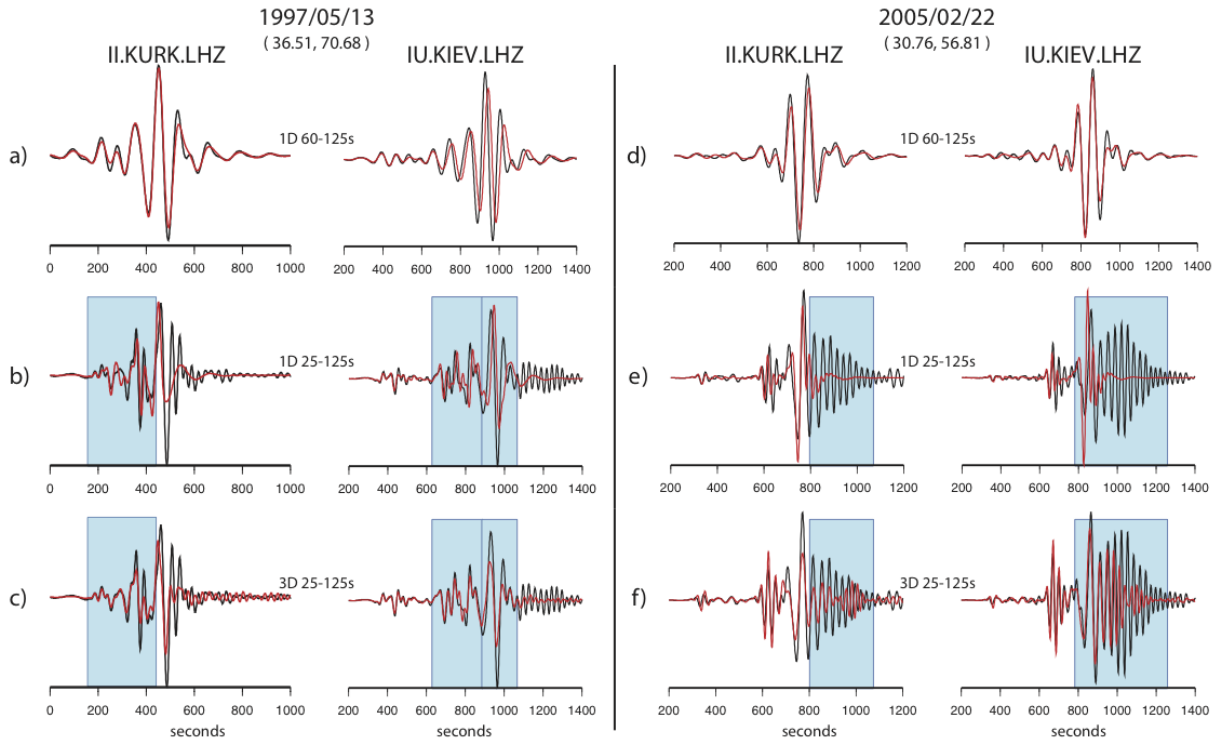

Figure 2. Comparison Between 1D and 3D Wave Speed Models at Long and Short Periods

Figure 2 demonstrates the need to use an initial 3D wave speed model as opposed to a 1D model as the starting point for the adjoint inversions. While the 1D model was used as a testbed to develop the procedures to accomplish the MT inversion, the synthetics and their prediction of the data at long and short periods is important. At long periods, 60-125 s, top row of Figure 2,

the 1D and 3D (not shown) wave speed models perform equally well at data reproduction. The primary arrivals at this period are the fundamental mode surface wave and very long period body waves. However, using the same model, synthetics, and data but at a shorter period, middle row of Figure 2, highlights the deficiencies in the 1D wave speed model. Again, the fundamental mode of the surface wave, the largest amplitude and longest period arrival, is well fit by the 1D wave speed model, but higher mode and shorter period surface waves are completely unaccounted for by the 1D model. Event 2005/02/22, right columns of Figure 2, demonstrates the lack of predicting power for the shorter period surface waves highlighted in the blue boxes. In contrast, the 3D wave speed model of the same events does much better at matching the dispersion and reproducing the amplitudes of the surface waves. Body waves at shorter periods are also matched much better by the 3D wave speed model. The left columns of Figure 2, for event 1997/05/13, show that synthetics based on the 3D model better fit the body wave (blue boxes) phases and amplitudes than do synthetics based on the 1D model.

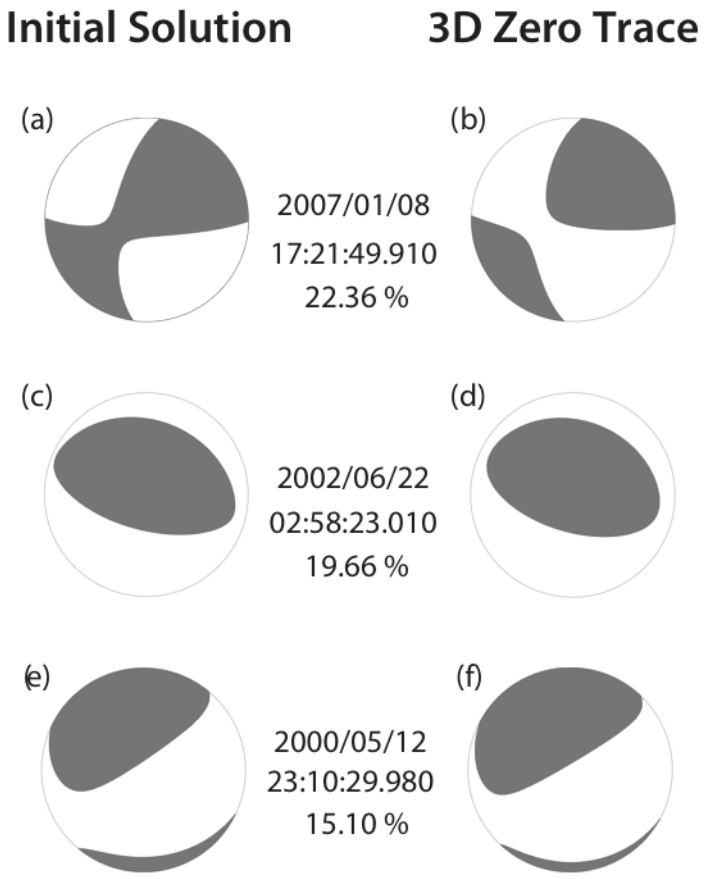

Figure 3. Comparison of the MT Solutions From Initial to Final Solutions

As stated above, the use of a 3D model at shorter period is essential for the adjoint inversion. This is due to a major reduction in computational cost as the a 3D initial model is about 7 adjoint iterations further along than a 1D initial model. Inversions for the MT also

benefit greatly from the vastly improved 3D model because 1) the inversion is able to use shorter period data and 2) use much more of the full waveform than possible with a 1D model. Use of better-predicted, shorter period data is important for MT inversions especially for stations near nodal planes of the MT. Amplitudes of arrivals near the nodal planes can be quite small, can change rapidly, and have the largest impact (largest derivatives) on the MT solution, as such the shorter period data allows the exploitation of these smaller amplitudes. As seen in Figure 3, our solutions are quite close to the original solutions derived from long period, teleseismic arrivals, but use of the shorter period data and nodal stations allows for a large variance reduction improvement over the original MT solutions. Minor changes in the MT solution, Figure 3, can have large impacts on nodal stations that ultimately drive large changes in variance reduction. Figure 3 includes three different MT solutions, which demonstrate our ability to recover the MT solution with our methodology.

Full seismic waveform data was used to accomplish the MT inversion with time window selection from the FLEXWIN tool [6] based on a set of relaxed constraints, detailed in [5]. A variety of inversions were performed to assess the impact of station distribution and the level of constraint on the final solution. While [5] reports solutions for 6 independent seismic moment tensor elements (Mij, zero-trace) plus depth, solutions using weaker or stronger constraints are consistent across inversion parameterization. To assess the errors in the inversion, we implemented a bootstrap procedure that randomly selects the different seismic stations to include in the inversion. As the inversion is quite fast, we are able to easily implement the bootstrap at minimal computational cost and obtain estimates of the standard error of the solutions. To evaluate the stability and consistency of each event, the P-axis of the MT is used as it provides a set of two numbers, i.e. trend and plunge, rather than six numbers, Mij, to compare. To note, the T-axis of the MT shows similar behavior to the P-axis allowing this reduction.

2.2. Adjoint Tomographic Inversion

Using the re-characterized events and seismic waveform data from Section 2.1, the wave speed model was improved using an adjoint tomographic inversion procedure. The inversion procedure is iterative so substantial improvement over traditional inversion procedures is possible and also allows continued improvement of a 3D wave speed model. The adjoint inversion is built upon the ability to localize errors within a wave speed model that manifest as mismatches between real data and synthetic seismograms from the current iteration wave speed model. The inversion procedure is a four step process: 1) create synthetic seismograms for the current wave speed model [7], 2) create adjoint sources from metrics between the data and synthetics [1], 3) use adjoint sources and the back-propagated, synthetic wavefield from step 1 to localize and quantify errors in the model [8], 4) update the model by minimizing the errors in the model and continue the iterations. Updates to the Middle East model were focused on improving the wave speeds and the adjoint sources were constructed to emphasize this.

Synthetics seismograms are generated in step 1) using the SPECFEM3D global package [7]. This earthquake simulation tool is able to generate synthetic seismograms from 3D wave speed, attenuation, and anisotropic models including effects of gravitation, rotation, topography, and bathymetry. Included within the package is the ability to save the final set of time-steps necessary to accomplish the back-propagation or time reversal in step 3).

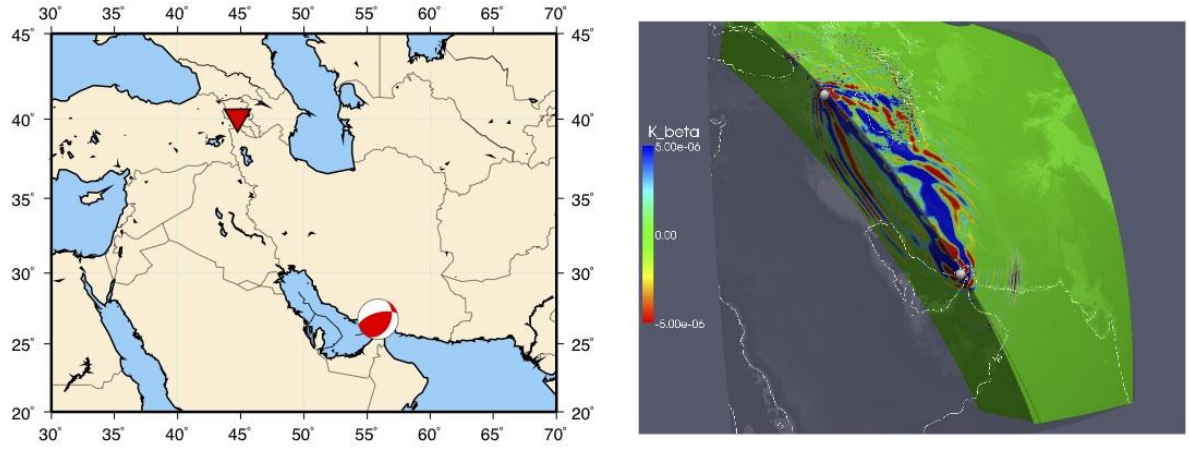

Figure 4. Single Station–Event Frechet Kernel Computed in a 3D Wave Speed Model

To create the adjoint sources in step 2), automatic measurements are made between the data and synthetics from SPECFEM3D using the FLEXWIN tool [6], creating data windows and associated metrics. Windows, and their adjoint sources, are not constrained to any specific seismic phase or time window and only use well matched data-synthetic pairs. In step 3) adjoint sources (step 2), a time series, along with the reconstructed, full synthetic wavefield (step 1) are propagated in reverse time through the current iteration wave-speed model to identify locations in the model requiring improvement. Figure 4 shows an example Frechet kernel derived from mismatches between data and synthetic seismograms from one event to one station, using two horizontal and the single vertical component. For reference, Frechet kernels derived from 1D models resemble simple banana-doughnut structures for longer period body waves. The kernels displayed in Figure 4 are more complex due to the presence of 3D structures and the use of the full wavefield, including body and surface waves. Interactions between the adjoint sources and the time-reversed wavefield, integrated over time, generate these kernels specific to each measurement, e.g. a simple difference between the data and synthetics. Such kernels can be created using individual, isolated measurements (Figure 4) or for each event with a large number of back-propagated adjoint sources (Figure 5).

The kernels derived using full-waveforms and a 3D wave speed model still resemble the traditional banana-doughnut shape, but have been modified by the interactions of multiple Frechet kernels from individual arrivals, and much more severely because of the use of a 3D wave speed model. Appearance of a number of "caustics" in the single event-single station kernel in Figure 4 are caused by either sharp changes in the current wave speed model or more likely structures existing in the Earth but unaccounted for in the 3D wave speed model. Large values in the kernel such as the Arabian Sea south of the event and the southern extent of the Caspian Sea are a result of large amplitude arrivals in the data that are missing in the synthetics. This mismatch is emphasized in the construction of the adjoint sources that are then back-propagated with the original wavefield to identify these two locations. The Caspian Sea kernel excursion is most likely due to thickened sediments, > 12km, in the southern Sea, while the southern Arabian Sea anomaly is a reflection from the ocean-continent boundary. Moreover, larger scale anomalies spread or smeared over the Frechet kernel normally indicate a overall

wave speed mismatch between the true model, the real Earth, and the current 3D wave speed model.

Event kernels, similar to Figure 4 but with more stations, are then summed volumetrically to produce Fréchet derivates, Figure 5, that are used to update the wave-speed model to complete step 4 and a single iteration. The process is then restarted, or iterated on, to continually improve the 3D model. As a consistency check, a small subset of events, ~5%, are not included within the inversion process, but synthetics are calculated and metrics for the evaluation windows are derived. Figure 5 shows 5 event kernels summed together. The individual events' kernels are identifiable in the right side of Figure 5 as large values in the Frechet derivative. A good example of the large values near the source is the event to the east of the southern Caspian Sea. The event creates an inverted "U" shape on the surface surrounding the source.

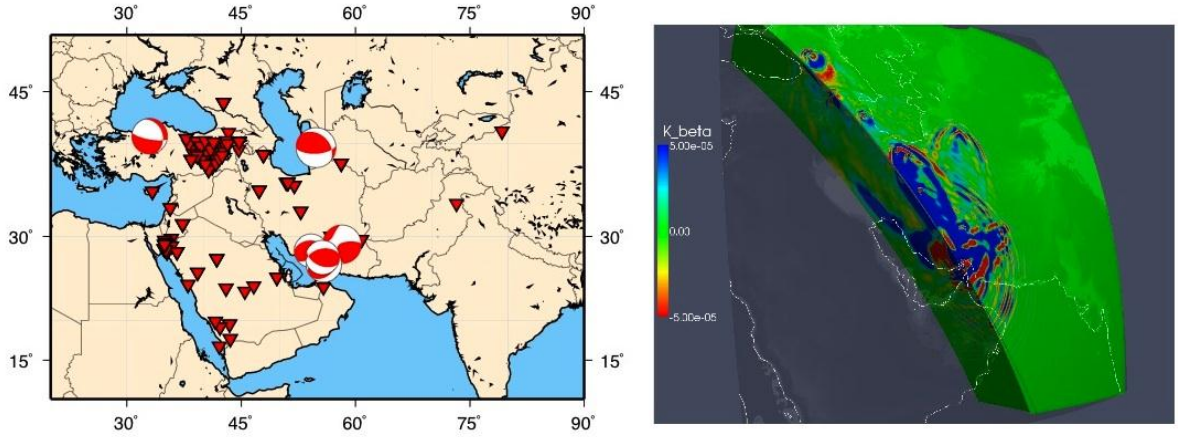

Figure 5. Multiple Station-Event Frechet Kernel Computed in a 3D Wave Speed Model

3. RESULTS AND DISCUSSION

3.1. Event Re-characterization

The comparison between Global CMT solutions and the MT solutions presented here show negligible differences in source mechanisms as measured from the P-axis. This is true for all cases (1D vs 3D model, minimum period 25s vs 60s) examined and when varying constraints are applied to the inversion [5]. In all cases, a reduction in variance between data and synthetic is seen between the original solution and our calculated solutions. The greatest reduction in variance is seen in the 3D case when filtered between 25-125s. A majority of events see a variance reduction of 5-40%, which represents a significant improvement in fitting waveforms. The largest variance reductions are a result of a better amplitude agreement between the data and synthetics.

To assess the robustness of the MT solutions we implemented a bootstrap procedure to determine the solutions' standard errors. We use the orientation, trend, and plunge of a MT's P-axis to quantify its error. For all of our events, the P-axis distributions are similar to the T-axis

distributions. For two events the trend of the P-axis is shown in Figure 6 where results from the 1D wave speed model are shown as an outlined histogram and the 3D wave speed model is the gray histogram. Also included in Figure 6, are the lower hemisphere projections of the P-axes for all bootstrap runs for the selected events. A tighter cluster of points indicates a smaller error in trend and plunge of the P-axis and of the MT solution overall. For all events, the P-axis has a larger standard error in trend than in plunge. This can be seen as the cluster of points is normally smeared along circles tangential to the bounding circle, see Event 1997/05/13 1D. P-axes were corrected for 0/360 crossing and plunges near horizontal using a simple analysis to find the smallest standard error by forcing the P-axes to be within a similar reference frame.

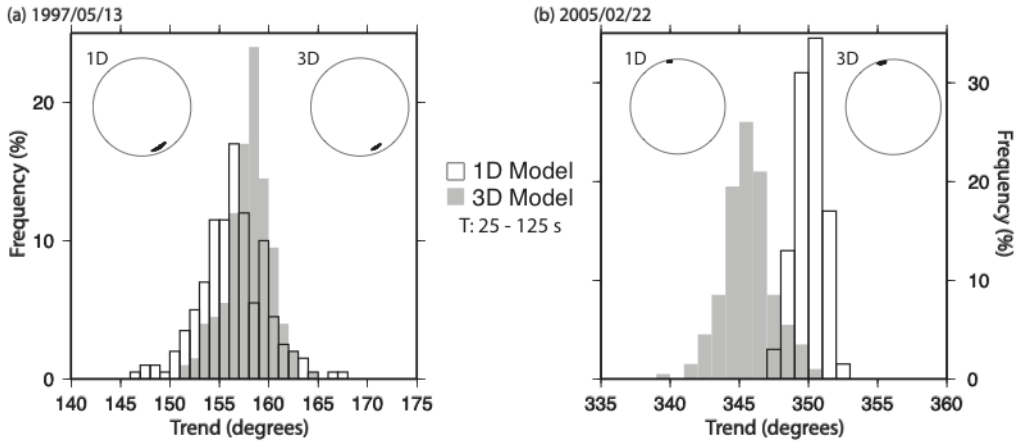

Figure 6. Results of the Bootstrap Procedure to Determine Standard Errors for Two Events

The largest contribution to the misfit in our result can be attributed to poorly constrained, shallow Earth structure. The use of shorter periods (25-125s) introduces a potential for contamination from larger errors due to unresolved wave speed structures. At shorter periods, Earth structure will have a greater influence on the propagating wavefield and errors in the Earth model may be mapped into the source solution. There is a small, but significant, increase in standard error on the trend and plunge of the P-axis (or T-axis) as well as a decrease in the average cross-correlation value from 60-125s to 25-125s (Figure 7). We do not feel the degradation in solution stability, as seen by the increase in trend and plunge standard error, and waveform metrics, as seen by the decrease in the cross-correlation value, are justification for the removal of shorter period signal. Alternatively, the addition of shorter period signals, 25-125s, allows for much more seismic data to be incorporated into the inversion indicating a robust predictive capability of the 3D wave speed model over a wide period range. An azimuthal gap in seismic stations seen in Kazakhstan and Russia also contributes to the error of the trend of some solutions, but for most events the overall azimuthal coverage is excellent and the trend is well constrained for the entire data set as a whole when using the 3D moment tensor inversion.

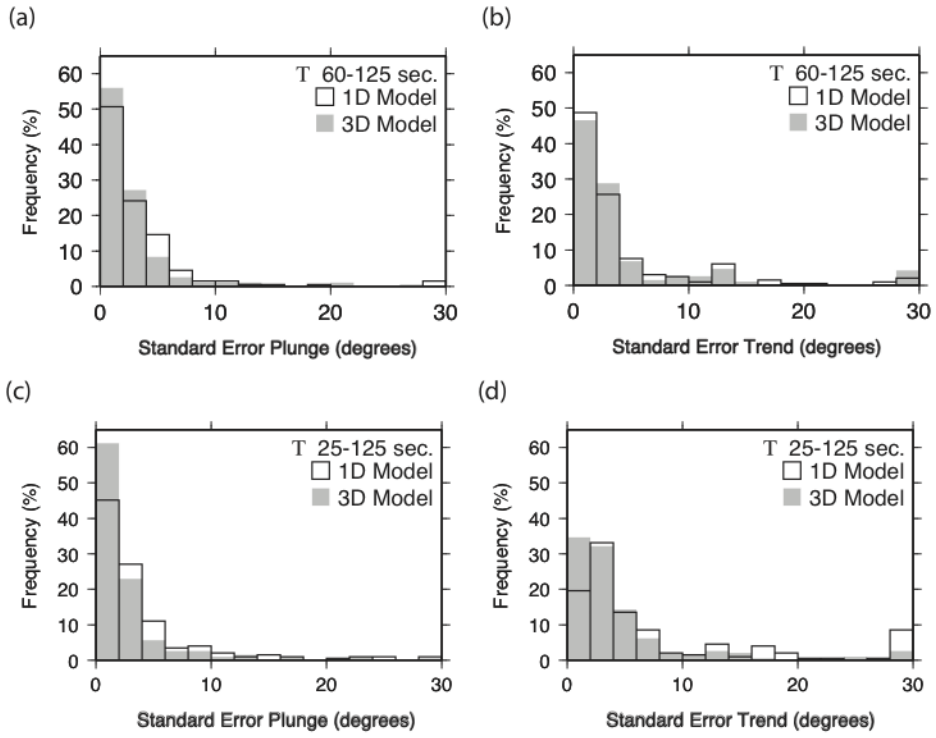

Figure 7. Standard Error for the P-axis of the Moment Tensor

Event depth is an essential variable when undertaking the adjoint tomographic inversion. Our results for depth when compared to the original solution depth are shown in Figure 8. Minor changes in depth, especially for shallow events, can severely modify the resulting waveforms, and errors in the simulated depth can be mapped directly into errors in the resulting 3D, adjoint wave speed model. If errors in depth are allowed to be mapped into the adjoint model they can substantially affect the absolute wave speeds, amplitude predictions, attenuation measurements, and result in larger standard errors of the final model. In Figure 8 we compare our inversion for depth with the original depth. Our results compare quite well when using a 3D wave speed model at all period ranges. As with the P-axes, we performed a bootstrap analysis to determine the standard error for the event depth. For all events, the standard error is smaller than the symbol size in Figure 8. Results at periods between 25-125 s, higher frequency, are more consistent with the original depth than those at 60 - 125s, low frequency. There is some discrepancy at depth around 100 km for the longer period solutions. This variability might be due to how the initial solutions are constructed and/or a more limited depth resolution at longer periods. Variability is also apparent at the shallowest depths. The initial solution has a depth minimum at 15 km whereas our solutions are allowed to vary throughout the crust. As expected, many of the shallowest events that were originally set at 15 km have been revised to shallower depths. Further, the use of shorter period arrivals produces more consistent depths than the longer periods solutions.

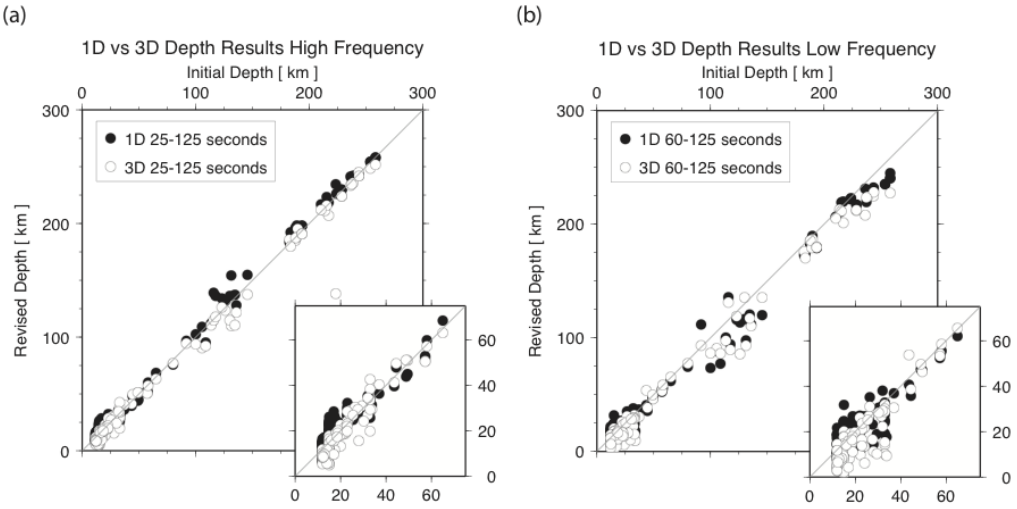

Figure 8. Comparison Between Original and Update MT Solution Depth

3.2. Adjoint Tomographic Inversion

Improvements in the wave-speed model for a sample set of iterations is shown in Figure 9 as changes in the traveltime and in Figure 10 as absolute shear wave speeds, Vsv and Vsh. The incorporation of transverse isotropy, also known as polar anisotropy, Vsv and Vsh, is essential for solution stability in the mantle. Figure 9 demonstrates the improvement in the wave speed model manifested as misfit between data and synthetics seismograms. The gray histograms are a previous inversion and the colored histograms are the improved model. Identification of body wave and surface waves are defined by the absolute wave speed of the arrival at a station.

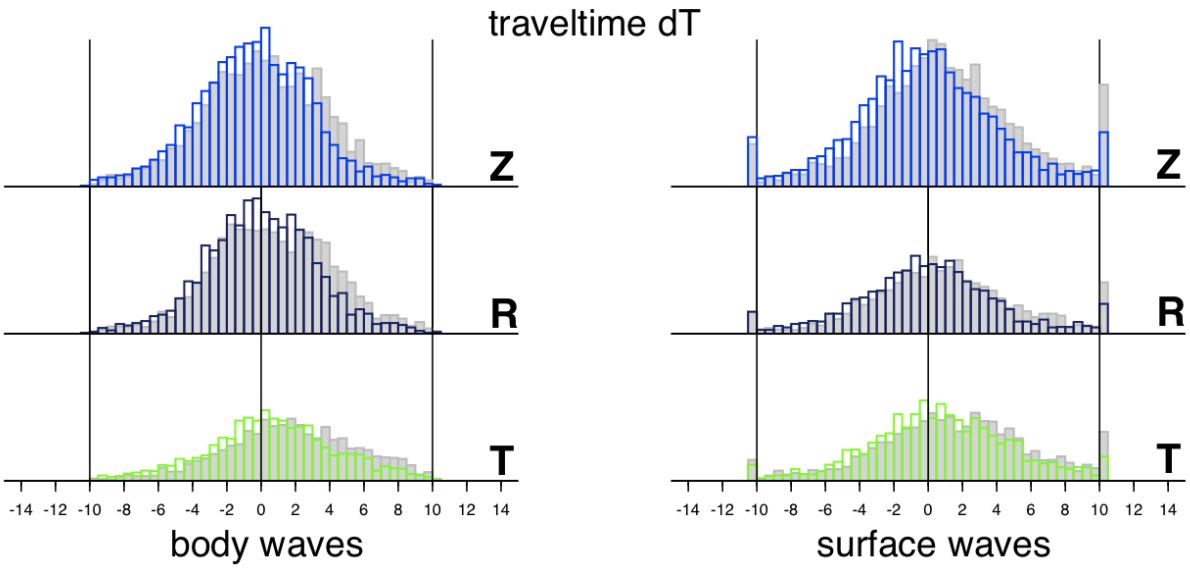

Figure 9. Improvements to the Traveltime, dT, Metric at Select Model Iterations

A majority of the improvement in the model is on the vertical and radial components as measured by traveltime, indicating an larger improvement to the vertical shear wave speed in the mantle over the horizontal shear wave speed. Improvements are equally divided between body and surface waves demonstrating a well-balanced inversion procedure that does not emphasize one type of arrival over another. This is primarily a result the adjoint source creation that normalizes the amplitude of arrivals and relies on the relative misfit of an arrival rather than the absolute amplitude. Moreover, the inversion is dominated by misfits in traveltime over amplitude misfit. This combination of the body and surface waves should produce a more robust

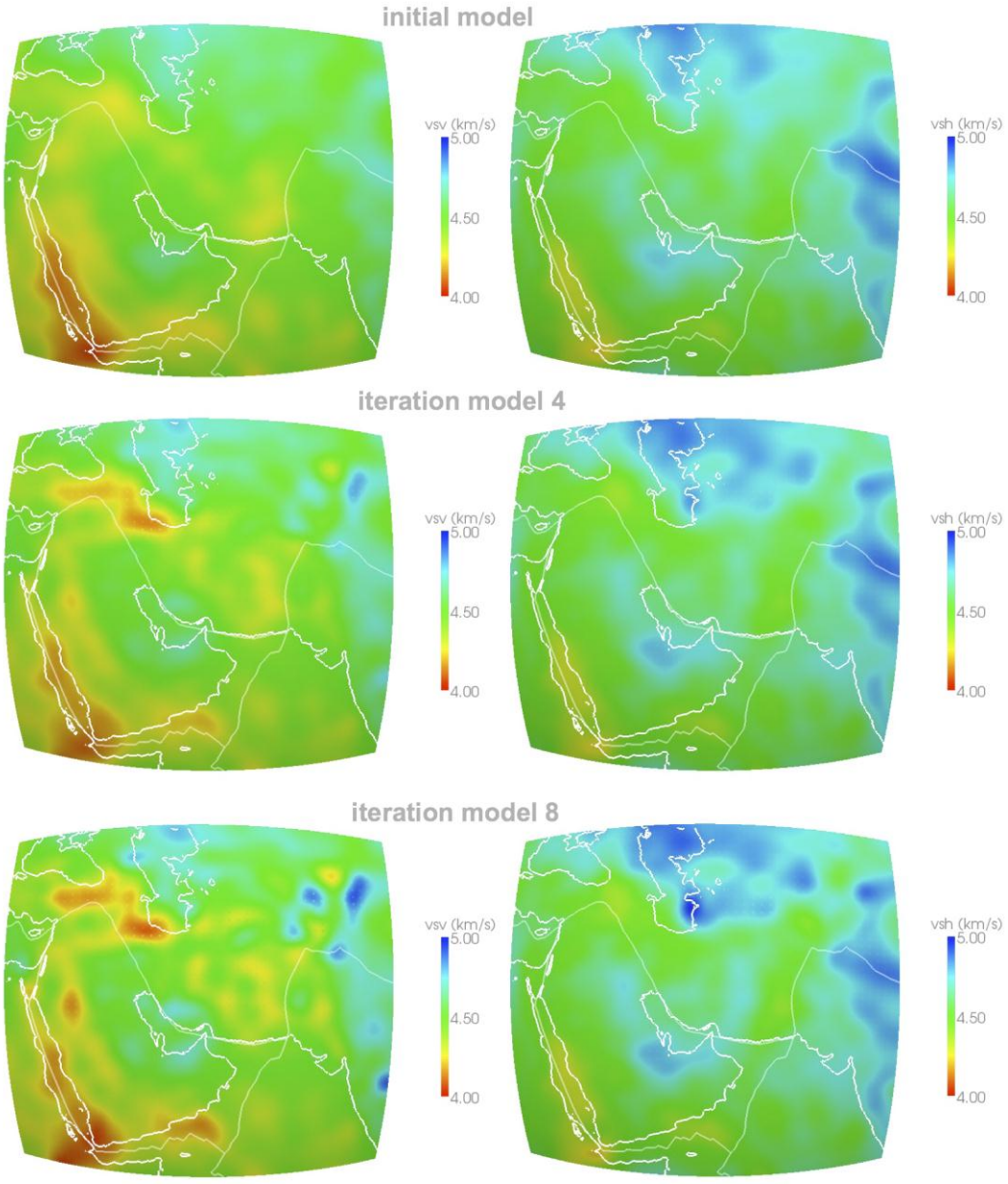

Figure 10. Comparison of the Middle East Wave-Speed Model at Different Iterations

model that has a greater predictive power over a 3D wave speed model derived from a single data source. Along with the improvement of traveltime metrics, amplitude misfits are slightly improved. This minor improvement indicates that either the bending of wavefronts at the current minimum period are not important or the long-wavelength, anelastic attenuation structure is reasonably characterized in the model. The progression to shorter periods will begin to incorporate both wavefront bending and anelastic attenuation in a more dramatic fashion. As the iterations continue to localize wave speed structures, the possibility of severe wavefront bending becomes a greater possibility. Moreover, as even-more shorter period arrivals are incorporated into the inversion, anelastic attenuation and variations within will more dramatically affect the amplitudes of these arrivals, necessitating the need to improve the anelastic attenuation model.

As the number of iterations increases, improvements are applied to the model and shorter period data are included in the inversion. With these improvements and shorter period data higher resolution structures begin to appear in the wave-speed model. Two examples of new higher resolution structures are in the Red Sea in Vsv and in the South Caspian Sea in Vsh. It is interesting to note the wave-speed model prefers reductions in wave speed in Vsv and increases in wave speed as Vsh; a feature that would not be possible without transverse isotropy in the mantle and the fitting of both Love and Rayleigh waves.

The incorporation of anisotropy was essential for stability of the inversion for wave speeds in the upper mantle. The simplest parameterization of transverse isotropy with a vertical symmetry axis allowed for inversion stability and imaging of the large wavelength structure of the ocean and continent. Inclusion of shorter period arrivals will begin to show the limitations of this anisotropic parameterization. Work by [9] indicates anisotropy beneath the ocean that is well characterized by global flow models except in regions of upwelling and downwelling. In contrast, the continents require an understanding of the geologic strain history to accurately define the total amount of strain and thus the anisotropy. In essence, the oceanic mantle can be well-characterized by horizontal flow and a transverse isotropy with a vertical symmetry axis, but the continents and regions with vertical mantle flow require a more complex treatment of anisotropy appropriate for the direction of mantle flow or, in the case of the Middle East, the preserved strain history of the Asian, Arabian, and Indian tectonic plates. Without knowing the true lateral changes in anisotropy and including large continental provinces within the model it is most appropriate to parameterize the mantle with a more general form of anisotropy to accurately resolve the wave speed structures.

A set of comparisons, waveforms and cross-sections, between the current iteration and the starting model (S2.9EA) are contained in Figure 11. Waveform fits from a path from the southern Zagros to station KBK demonstrates that updates to the model are improving the fit between data and synthetics. As mentioned before, this event is not included in the adjoint tomography, but is used to provide a consistency check on the model improvement and progression. After about a third of the total iterations, a lower wave speed Vsv lithosphere is required in the middle of this path, to the southwest of Tibet's western syntaxis. This lower wave-speed region appears in the cross sections, but is also apparent in the synthetics. The surface wave in the starting model arrives earlier than the data, but arrives "on-time" using the current iteration model.

Updates to the model also include density and compressional components. The initial 3D compressional wave-speed model was scaled in the initial model from the 3D shear wave speed

by a constant factor. Shear wave speeds in S2.9EA were derived from a large number of Love, Rayleigh, and shear body wave arrivals. A comparison between the compressional adjoint results and the initial model can be difficult as the ratio between shear and compressional wave speeds can vary due to composition. All adjoint iterations for compressional wave speeds show a much slower upper mantle beneath much of the Middle East than indicated by S2.9EA. Updates to the model at long wavelengths for these initial iterations are predominately controlled by Rayleigh waves (shear and compressional surface wave) as the initial S2.9EA model fit the Love waves (shear only surface waves) better (Figure 11).

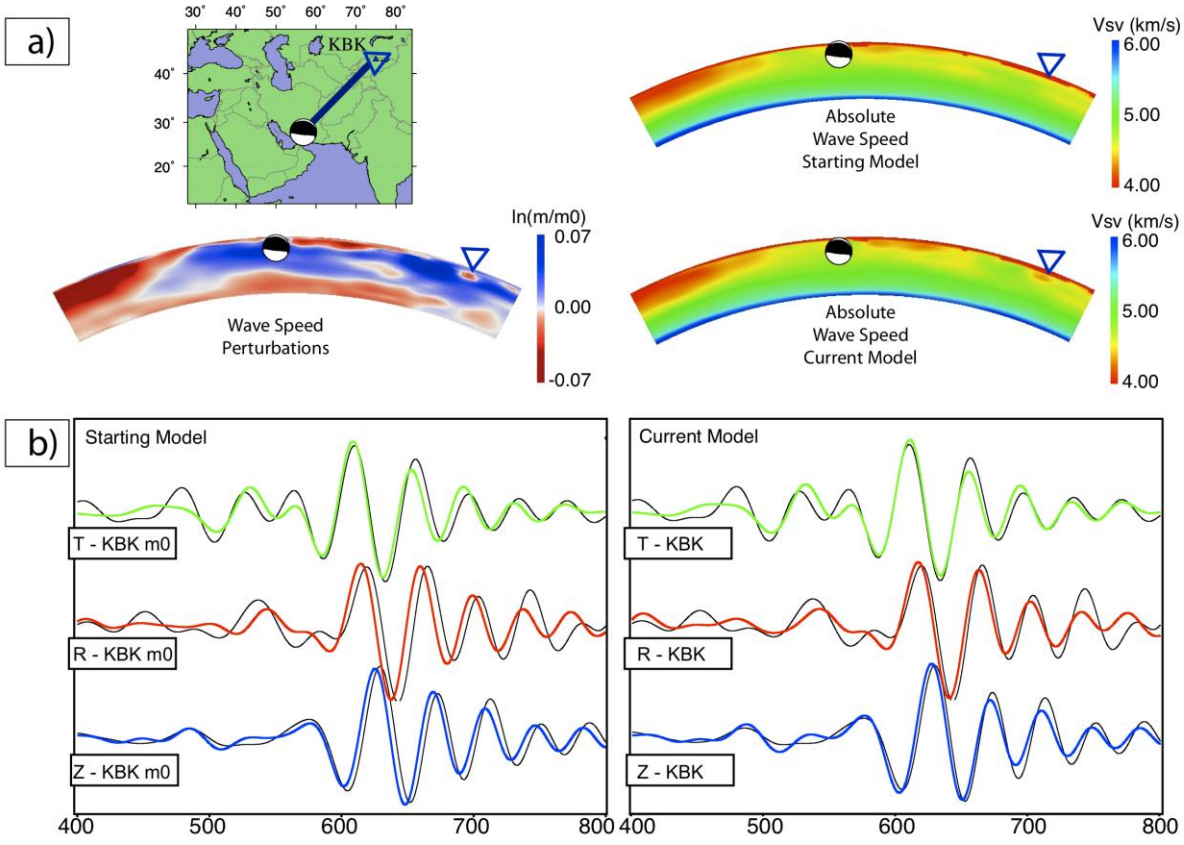

Figure 11. Demonstration of the Current Iteration Model Through a Single Station – Event Pair

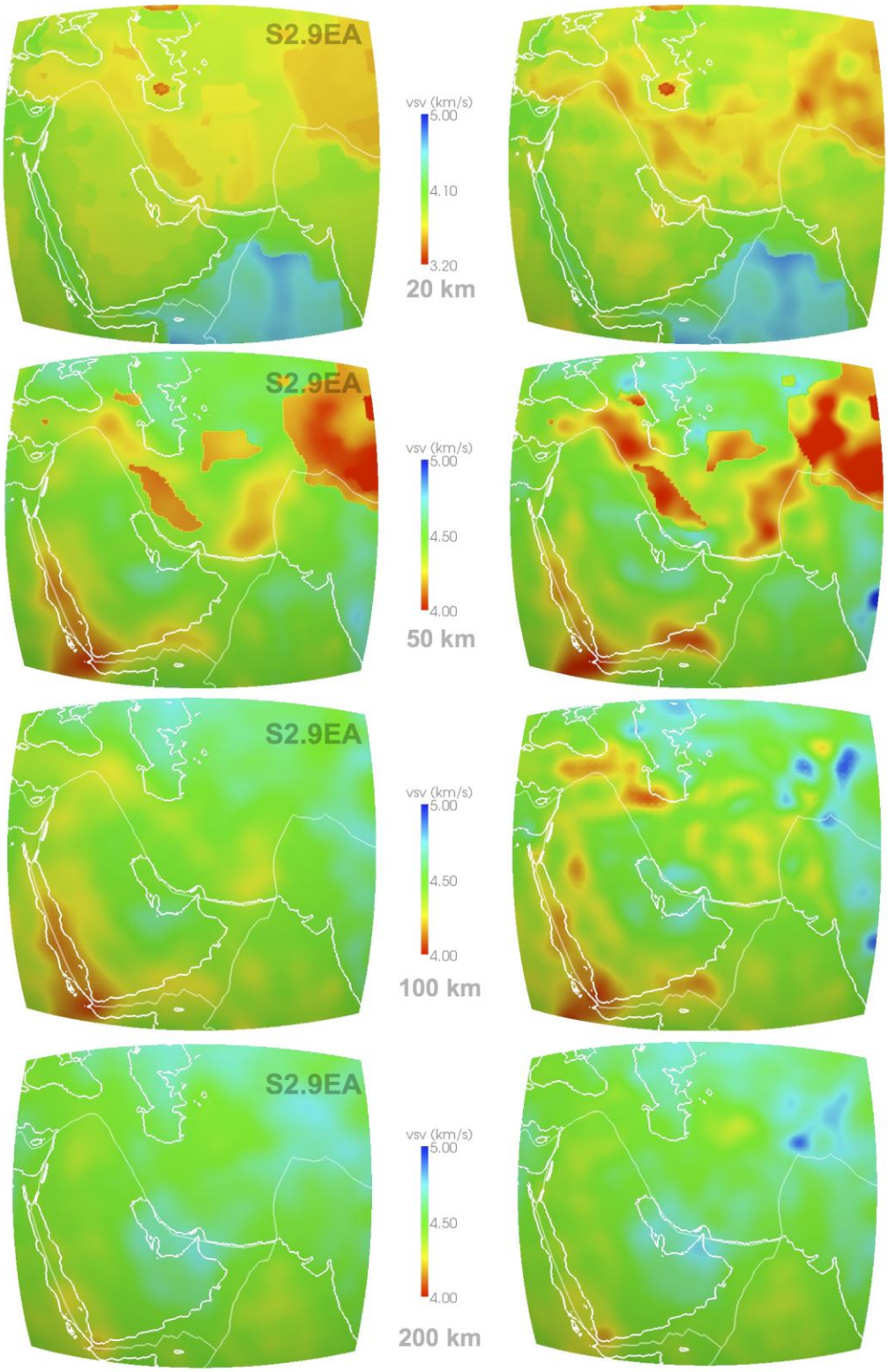

Figure 12. Absolute Vsv Speeds, Initial vs Final Model, Presented at Selected Depths

Figure 12 shows a comparison between the Middle East 3D wave speed model from the initial model to the final model. Shown is the vertical shear wave speed, which is sensitive to misfits from Rayleigh waves and to a lesser extent body waves. The overall pattern of the anomalies does not change from the initial to the final model, but the absolute magnitude and the shape of the anomaly is significantly changed. As the iterations progress, anomalies spatially shrink, but increase in overall magnitude, thus localizing the structures. Examples of this structure localization can be identified at 50 km in western Tibet and south of the Black Sea at 100 km. Further, artifacts from the initial 3D wave speed model due to either poor sampling in a region or ambiguous structures not resolvable using traditional inversion techniques are diminished in amplitude. Examples of artifact removal are at 50 and 100 km to the west of the Persian Gulf.

4. CONCLUSIONS

Adjoint iterations to update the wave-speed model of the Middle East have shown dramatic improvements based on data / synthetic comparisons and expected behavior when introducing a finite-frequency tomographic approach. Before iterations began, a seismic waveform database with ~200 reinterpreted sources in the Middle East was compiled to avoid the mapping of source errors into wave-speed structure [5]. All sources in the database agree with previously published solutions and between the methodologies used: CAP [9], teleseismic [10], and a MT inversion [2]. Initial comparisons between data and synthetics computed from the initial 3D model S2.9EA [4] at 25 seconds and longer show reasonable agreement and a general improvement over the 1D PREM model [3].

To further improve the fit between data and synthetics, the adjoint tomographic inversion methodology was implemented to iteratively update the 3D wave-speed model [1]. The wave-speed model was parameterized to incorporate transverse isotropy in the mantle to accommodate the simultaneous fitting of Rayleigh and Love waves and stabilize the inversion in the upper mantle. As the model progressed through a series of iterations, regions of wave-speed anomalies increased in strength from the initial to the current iteration as physics of wave propagation were incorporated into the inversion; see, e.g., the Red Sea and the southern Caspian Sea, Figures 10 and 12. Compressional wave-speed estimates also improved from increased use of Rayleigh waves. The final model fits body waves down to a minimum period of 14 seconds and surface waves to a minimum period of 20 seconds, and the wave-speed model is able to resolve wave-speed features with scale lengths of 60 km. Our recommendations for a robustly constrained 3D wave-speed model in the Middle East include using quality controlled seismic waveform data from well-constrained sources and use of a physics based tomographic technique to improve upon existing 3D models. Further recommendations to improve the wave-speed model include adding:

- anisotropic effects where necessary, e.g. the mantle, and
- attenuation to improve fits to amplitudes, and
- shorter period signals to further improve the waveform predictive capabilities of the wave-speed model of the Middle East.

REFERENCES

[1] Tromp, J., C. Tape, and Q. Liu, "Seismic tomography, adjoint methods, time reversal and banana-doughnut kernels," *Geophysical Journal International*, **160**(1), 2005, pp. 195–216.

[2] Liu, Q., J. Polet, D. Komatitsch, and J. Tromp, "Spectral-Element Moment Tensor Inversions for Earthquakes in Southern California," *Bull. Seism. Soc. Am.*, **94**(5), 2004, pp. 1748–1761, doi:10.1785/012004038.

[3] Dziewonski, A., and D. Anderson, "Preliminary reference Earth model," *Phys. Earth. Planet. Int.*, **25**, 1981, pp. 297–356.

[4] Kustowski, B., G. Ekstrom, and A. Dziewonski, "The shear-wave velocity structure in the upper mantle beneath eurasia," *Geophysical Journal International*, **174**, 2008, pp. 978–992, doi:10.1111/j.1365-246X.2008.03865.x.

[5] Covellone, B. M., and B. Savage, "A Quantitative Comparison Between 1D and 3D Source Inversion Methodologies: Application to the Middle East Region," *Bull. Seism. Soc. Am.*, 2012, in review.

[6] Maggi, A., C. Tape, M. Chen, D. Chao, and J. Tromp, "An Automated time-window selection algorithm for seismic tomography," *Geophysical Journal International*, **178**(1), 2009, pp. 257–281, doi:10.1111/j.1365-246X.2009.04099.x.

[7] Komatitsch, D., and J. Tromp, "Introduction to the spectral-element method for 3-D seismic wave propagation," *Geophysical Journal International*, **139**, 1999, pp. 806–822.

[8] Tape, C., Q. Liu, and J. Tromp, "Finite-frequency tomography using adjoint methods - Methodology and examples using membrane surface waves," *Geophysical Journal International*, **168**(3), 2007, pp. 1105–1129.

[9] Conrad, C., M. Behn, and P. Silver, "Global mantle flow and the development of seismic anisotropy: differences between the oceanic and continental upper mantle," *Jour. Geophys. Res.*, **112**(B07317), 2007, doi:10.1029/2006JB004608.

[10] Zhao, L., and D. Helmberger, "Source estimation from broadband regional seismograms," *Bull. Seism. Soc. Am.*, **84**(1), 1994, pp. 91–104.

List of Acronyms

AFRL	Air Force Research Laboratory
MT	Moment Tensor

DISTRIBUTION LIST

DTIC/OCP
8725 John J. Kingman Rd, Suite 0944
Ft Belvoir, VA 22060-6218 1 cy

AFRL/RVIL
Kirtland AFB, NM 87117-5776 2 cys

Official Record Copy
AFRL/RVBYE/Robert Raistrick 1 cy